PERPUSTAKAAN UMP
0000096933

Surface Characterization and Biocompatibility of Nanostructured TiNi Alloys Processed by High-Pressure Torsion

Dayangku Noorfazidah Binti AWANG SHRI
Doctoral Program in Materials Science and Engineering

Submitted to the Graduate School of
Pure and Applied Sciences
in Partial Fulfillment of the Requirements
for the Degree of Doctor of Philosophy in
Engineering

at the
University of Tsukuba

Table of Contents

Acknowledgements i

List of Figures vii

List of Tables x

Chapter 1 Introduction 1

1.1 TiNi Alloys 1

1.2 Biomaterials 3

1.2.1 Biomaterial and surface interaction 4

1.2.2 Protein adsorption 5

1.3 Surface Characterization 6

1.3.1 Surface characterization 6

1.3.2 X-ray Photoelectron Spectroscopy 6

1.4 Corrosion in biomaterial 8

1.4.1 General concept of corrosion 9

1.4.2 Corrosion resistance of TiNi alloys 11

1.4.3 Ni ion release 12

1.5 Severe plastic deformation 12

1.5.1 Equal-channel angular pressing (ECAP) 13

1.5.2 Accumulative roll bonding (ARB) 13

1.5.3 Multi-directional forging (MDF) 14

1.5.4 High pressure torsion 15

1.5.5 Parameter in estimating the strain in HPT 16
1.6 Research objectives 18
1.7 Thesis outline 18
1.8 References: 19

Chapter 2 Phase Analysis and Mechanical Properties Characterization of TiNi Deformed by High Pressure Torsion 23
2.1 Introduction 23
2.2 Experimental Procedures 24
2.2.1 Material preparation 24
2.2.2 Material characterization 24
2.3 Results 25
2.3.1 Structural Evolution 25
2.3.2 Mechanical properties 27
2.4 Discussion 27
2.5 Conclusion 29
2.6 References 30

Chapter 3 Biocompatibility of Nanostructured TiNi Processed by High-Pressure Torsion 31
3.1 Introduction 31
3.2 Experimental Procedures 32
3.2.1 Material preparation 32
3.2.2 Cell cultures 32
3.2.3 Cytocompatibility Evaluation 32
3.2.4 Nickel ion release 33
3.2.5 Protein adsorption analysis 33
3.3 Results 35

3.3.1 Colony formation and morphology 35
3.3.2 Ni ion release 37
3.3.3 Protein adsorption behavior 37
3.4 Discussion 40
3.4.1 Effect of HPT on the colony formation behavior 40
3.4.2 Suppression of Ni ion release by HPT deformation 40
3.4.3 Effect of HPT on the protein adsorption behavior 41
3.5 Conclusion 42
3.7 References: 43

Chapter 4 Surface characterization of HPT deformed TiNi alloys 45
4.1 Introduction 45
4.2 Experimental method 46
4.2.1 Sample preparation 46
4.2.2 X-ray photoelectron spectroscopy 46
4.3 Results 47
4.3.1 Surface characterization of Ti-50mol%Ni 47
4.3.2 Surface characterization of Ti-50.9mol%Ni 59
4.4 Discussion 67
4.4.1 Effect of HPT on the surface composition of TiNi 67
4.4.2 Effect of HPT on the TiNi passive film formation 68
4.4.3 Effect of cell culture to the passive film in TiNi 71
4.5 Conclusion 71
4.6 References: 72

Chapter 5 Electrochemical Characterization of TiNi alloys Deformed by High Pressure Torsion 75

5.1 Introduction 75

5.2 Experimental Methods 76

5.2.1 Sample preparation 76

5.2.2 Electrochemical measurements 76

5.3 Results 77

5.3.1 OCP Measurement 77

5.3.2 Polarization curves 78

5.4 Discussions 81

5.5 Conclusion 84

5.6 Reference 85

Chapter 6 Conclusions 87

List of Figures

Fig. 1.1 Schematic illustration of the crystal structure of TiNi (a) B2 cubic unit cell of austenite and (b) B19' monoclinic unit cell. 1

Fig. 1.2 Schematic representation of the shape memory effect of TiNi alloy [2]. 2

Fig. 1.3 Schematic representation of the superelasticity effect of TiNi alloy [2] 3

Fig. 1.4 Surface properties governing behavior of implanted material [8]. 4

Fig. 1.5 Schematic representation of the process of protein adsorption on a solid surface [14]. 6

Fig. 1.6 An electron energy diagram for a Ni^{2+} showing the absorption of a photon and resultant expulsion of a 2p level photoelectron 8

Fig. 1.7 Influence of fibroblast on the corrosion of biometallic material [37]. 12

Fig. 1.8 Schematic of ECAP process [48] 13

Fig. 1.9 Schematic of ARB process [49]. 14

Fig. 1.10 Schematic of MDF process [50]. 14

Fig. 1.11 Schematic illustration of HPT processing [52]. 16

Fig. 1.12 Parameters used in estimating the total strain in HPT. 17

Fig. 2.1 Schematic illustration of microhardness testing along the radial of the sample. 24

Fig. 2.2 (a) X-ray diffraction patterns of Ti-50mol%Ni before and after HPT deformation and (b) its corresponding FWHM at 2θ ~ 42° 25

Fig. 2.3 (a) X-ray diffraction patterns of Ti-50.9mol%Ni before and after HPT deformation and (b) its corresponding FWHM at 2θ ~ 42° 26

Fig. 2.4 Micro-hardness of (a) Ti-50mol%Ni and (b) Ti-50.9mol%Ni before and after deformation with different turns as a function of distance from the disk center. 27

Fig. 2.5 Schematic illustration of the nanostructures of HPT deformed TiNi as observed by TEM showing the nanograins (black) and amorphous (gray)region [17]. 29

Fig. 3.1 Giemsa-stained samples showing the colony on the Ti-50mol%Ni samples surfaces. 33

Fig. 3.2 SEM images of BHPT Ti-50mol% showing the negative and positive control. 34

Fig. 3.3 Representative image showing colony morphology formed on the surface of (a) BHPT (b) N = 0.25 (c) N = 0.5, (d) N = 1, (e) N = 5 and (f) N = 10 Ti-50mol%Ni samples 36

Fig. 3.4 Representative image showing colony morphology formed on the surface of (a) BHPT (b) N = 0.25 (c) N = 0.5, (d) N = 1, (e) N = 5 and (f) N = 10 Ti-50.9mol%Ni samples 36

Fig. 3.5 Plating efficiency of (a) Ti-50mol%Ni and (b) Ti-50.9mol%Ni. 37

Fig. 3.6 Ni ion release from (a) Ti-50mol% Ni and (b) Ti-50.9mol%Ni as a function of HPT rotation. ... 38

Fig. 3.7 (a) Albumin and (b) vitronectin adsorption on Ti-50mol%Ni as function of HPT rotation. 39

Fig. 3.8 (a) Albumin and (b) vitronectin adsorption on Ti-50.9mol%Ni as function of HPT rotation. 39

Fig. 4.1 A representative survey XPS spectrum of (a) BHPT Ti-50mol% Ni and (b) BHPT Ti-50.9mol%Ni. 48

Fig. 4.2 Deconvolution of C1s peak on Ti-50mol% BHPT sample. 50

Fig. 4.3 Series of C1s peak of Ti-50mol%Ni (a) before and (b) after cell culture. 51

Fig. 4.4 Deconvoluted spectra of Ti 2p region of Ti-50mol%Ni BHPT sample. 52

Fig. 4.5 Deconvolution spectra of O 1s region of Ti-50mol%Ni BHPT sample. 52

Fig. 4.6 Series of O1s peaks of Ti-50mol%Ni (a) before and (b) after cell culture. 53

Fig. 4.7 Series of Ni 2p peaks of Ti-50mol%Ni (a) before and (b) after cell culture. 54

Fig. 4.8 Ratio of (a)$Ti^{[Me]}$ / $Ti^{[Ox]}$ and (b) $Ni^{[Me]}$ /$Ni^{[Ox]}$ as function of HPT rotation of Ti-50mol%Ni 55

Fig. 4.9 Series of N 1s peaks of Ti-50mol%Ni after cell culture. 57

Fig. 4.10 Depth profile for (a) BHPT, (b) N = 0.25 and (c) N = 0.25 before cell culture. 58

Fig. 4.11 Depth profile for (a) BHPT, (b) N = 0.25 and (c) N = 0.25 after cell culture. 58

Fig. 4.12 Series of C 1s peaks of Ti-50.9mol%Ni (a) before and (b) after cell culture. 62

Fig. 4.13 Series of O1s peaks of Ti-50.9mol%Ni (a) before and (b) after cell culture. 63

Fig. 4.14 Series of Ni 2p peaks of Ti-50.9mol%Ni (a) before and (b) after cell culture. 64

Fig. 4.15 Series of N 1s peaks of Ti-50.9mol%Ni after cell culture. 66

Fig. 4.16 Depth profile of Ti-50.9 mol%Ni for (a) BHPT, (b) N = 0.25 and (c) N = 0.25 before cell culture. 67

Fig. 4.17 Ratio of proportion of the metallic Ni to metallic Ti on the film oxide of Ti-50mol%Ni as the function of HPT rotation. 68

Fig. 4.18 Schematic illustration of passive film formation. 70

Fig. 5.1 Electrochemical cell setup used in this experiment. 77

Fig. 5.2 Open circuit potential of (a) Ti-50mol%Ni and (b) Ti-50.9 mol%Ni in cell culture media.......... 79

Fig. 5.3 The potentiodynamic polarization of (a) Ti-50mol%Ni and (b) Ti-50.9 mol%Ni in cell culture media. 79

Fig. 5.4 Surface morphologies of (a) microcystalline (b) amorphous and (c) nanocrystalline Ti-50.2mol%Ni after corrosion in Hank's solution [10]. 83

List of Tables

Table 2.1 Degree of torsional deformation with different number of revolutions (edge of sample) 27

Table 4.1 Chemical composition of the Ti-50 mol%Ni surface samples as measured by XPS 49

Table 4.2 Chemical composition of the Ti-50 mol%Ni surface samples as measured by XPS after cell culture 49

Table 4.3 Summary of contribution for each species from Ti-50mol% O1s and C1s spectra before and after cell culture 56

Table 4.4 Chemical composition of the Ti-50.9mol%Ni surface samples as measured by XPS 60

Table 4.5 Chemical composition of the Ti-50.9mol%Ni surface samples after cell culture as measured by XPS 60

Table 4.6 Summary of contribution for each species from Ti-50mol% O1s and C1s spectra before and after cell culture 65

Table 5.1 Corrosion parameter of Ti-50mol%Ni 80

Table 5.2 Corrosion parameter of Ti-50.9mol%Ni 80

Chapter 1 Introduction

1.1 TiNi Alloys

Titanium nickel (TiNi), an intermetallic compound, was discovered by metallurgist Willian J. Buehler at the Naval Ordinance Laboratory. The unique properties of an equiatomic TiNi alloys was discovered when he observed the major change in the atomic structure of the material due to temperature change [1]. The shape memory effect and superelasticity of TiNi alloys is attributed to its ability to exist in two different temperature-dependant phases: austenite and martensite. The high temperature austenite parent phase, stable under low stress is in cubic form with B2 structure. The low temperature martensite phase, stable under suitably higher stress condition, is monoclinic with B19' structure. Fig. 1.1 illustrates the crystal structure of B2 and B19'.

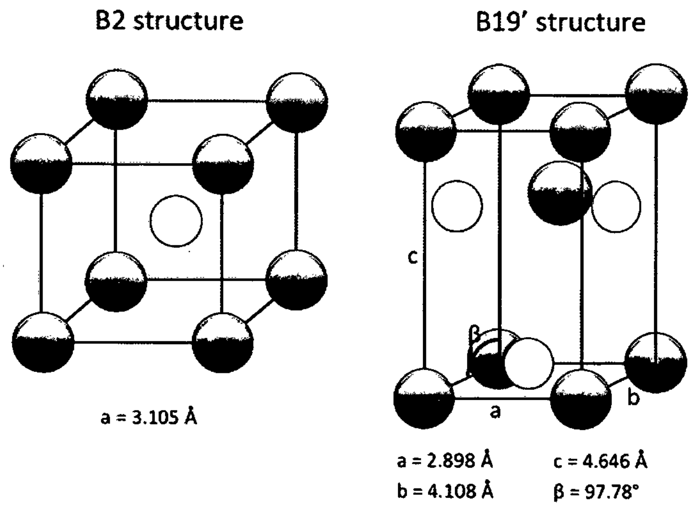

Fig. 1.1 Schematic illustration of the crystal structure of TiNi (a) B2 cubic unit cell of austenite and (b) B19' monoclinic unit cell.

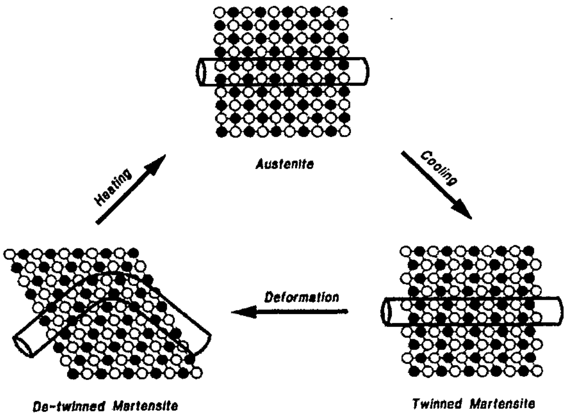

Fig. 1.2 Schematic representation of the shape memory effect of TiNi alloy [2].

The inherent ability of this alloy to alter their type of atomic bonding which causes unique and significant changes in mechanical properties and crystallographic arrangement is termed as superelasticity and shape memory effect. This changes, occurs as results of martensitic transformation, as a function of temperature and stress.

The mechanism of the shape memory effect is described as follows. Upon cooling, the austenite phase starts to transform to martensite at Ms (martensite start temperature). Since the martensite phase has lower symmetry than the austenite phase, martensites with the same structure but in different crystallographic orientations (called variants of martensite) can be formed. For example, in B2 (cubic) to B19' (monoclinic) transformation of Ni-Ti alloy, as many as 12 correspondence variants can be formed. Formation of martensite in the parent phase will cause a large strain due to the fact that the martensitic transformation is associated with a shape change. A combination of two or four variants may form in tandem to reduce this strain and this particular morphology is called self-accommodation. Variants in this morphology are twin-related to each other. Twins introduced upon martensitic transformation can act as a deformation mode if a stress is applied, since the twin boundary in Ni-Ti is mobile. This process is called detwinning as a favorably oriented variant grows at the expense of other less favorable ones. The deformation remains when the stress is released. Upon heating, the martensite variants revert to their original orientations in the austenite phase so that the original shape is restored. Ordinarily the shape memory effect is one-way as only the shape of the austenite phase is memorized.

Superelasticity at high temperatures is essentially due to a stress-induced martensitic transformation. When the SMA sample is at a temperature above Ms, in which the austenite phase is the dominant phase in a stress-free specimen, the martensite phase can be induced by application of an outer force. Once the stress is released, the martensite is unstable at high temperature, thus the reverse transformation happens and the strain is recovered. The high elasticity of NiTi is not simply stretching the atomic bonds, but it is the result of changes in the crystal structure by stress.

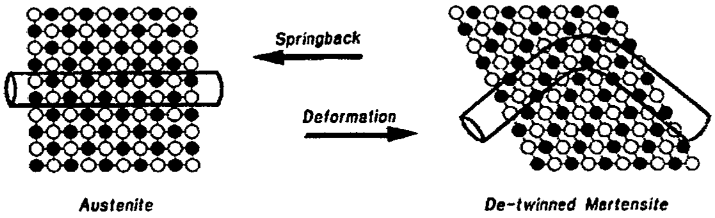

Fig. 1.3 Schematic representation of the superelasticity effect of TiNi alloy [2].

The superelasicity and shape memory effect of TiNi alloys made it one of the common metals used in the biomedical application such as orthodontic archwires, stents and guidewires. Superelasticity of TiNi alloys allows for the use as archwires as it can exert light and constant force on top of good mechanical properties and corrosion resistance [2,3]. For the usage as stent, TiNi stents are self-expanding, taking advantage of their shape memory capabilities. Their superelasticity allows for the delivery of stents to the intervention site without kinking or permanently deforming [4].

1.2 Biomaterials

Another consideration in the usage of TiNi alloys as medical devices is its biocompatibility. A biomaterial was defined by American National Institute of Health "as any substance (other than a drug) or combination of substances, synthetic or natural in origin, which can be used for any period of time, as a whole or as a part of a system which treats, augments, or replaces any tissue, organ, or function of the body" [5]. Since this definition excludes application such as orthodontic brackets and surgical instruments, the most appropriate definition for a biomaterials is proposed by D. F William as "material intended to interface with biological system to evaluate, treat, augment or replace any tissue, organ or function of the body" [6].

Biocompatibility is described as "the ability of a material to perform with an appropriate host response in a specific application"[6]. In order for a material to be deemed suitable for biological application, it must be fulfilled several requirements. The materials should be able to perform its biological requirement without causing any cell death, chronic inflammation or other damage of cellular or tissue function [7]. Besides the structural requirement, the biocompatibility also plays a crucial roles as the its surface is directly exposed to the living organism.

1.2.1 Biomaterial and surface interaction

The interaction between metal surfaces and tissues is a complex matter. In the long term, metal ions release from the surface and specific biological activity of these metal ions may affect the tissue adjacent to the metal implants. To understand the implication of the metal used as biomaterials, we have to first understand the interaction between biological environments with the material.

The outermost atomic layer of general biomaterial surface at the moment of insertion in to the tissue is a combination of inorganic or organic oxides and hydroxides with low chemical reactivity and low solubility at physiological conditions. Different surfaces possess different basic water chemistries as represented by their elemental compositions and functionalities, such as –OH, –CH3, PO4, –NH2, –COOH, and –SiOH groups. This chemistry also gives rise to different free surface energies, water-retaining capacities, surface mobility, and other properties that may or may not be important for blood and tissue responses. Fig. 1.4 summarizes a few important surface chemical and physical properties believed to be relevant to in vivo behavior of biomaterials [8].

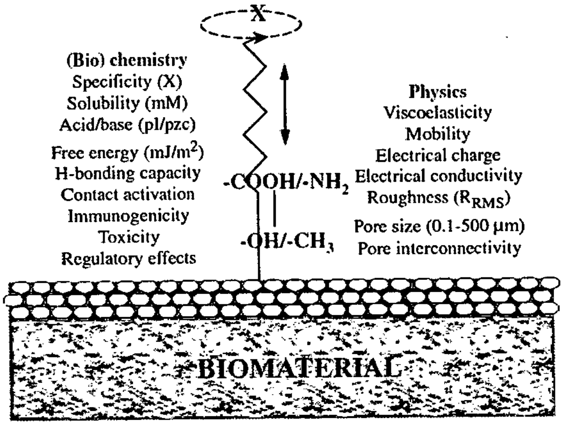
X
(Bio) chemistry
Specificity (X)
Solubility (mM)
Acid/base (pI/pzc)
Free energy (mJ/m^2)
H-bonding capacity
Contact activation
Immunogenicity
Toxicity
Regulatory effects
-COOH/-NH$_2$
-OH/-CH$_3$
Physics
Viscoelasticity
Mobility
Electrical charge
Electrical conductivity
Roughness (R$_{RMS}$)
Pore size (0.1-500 μm)
Pore interconnectivity
BIOMATERIAL

Fig. 1.4 Surface properties governing behavior of implanted material [8].

Biocompatibility of a material surface is closely related to the response of cells in contact with the surface and their adhesion. The initial response to a material placed in a biological environment is the adsorption of the water molecules. The extent and specific manner of interaction of the water molecules with the surface is dependent on the surface properties. These properties also determine the adsorption behavior of protein and other molecules. Within seconds to hours after implantation, adsorbed layer of protein covers the material surface. Then, the cells eventually reach the surface and interact with the surface through the protein layer [9]. Cellular responses are always mediated through proteins *via* their ligands [10]. The cells can adhere, release active compounds, recruit other cells, grow in size, replicate or die depending on their interaction with the adsorbed protein [11].

1.2.2 Protein adsorption

Proteins are essential parts of organisms and involve in many essential processes within cells. Proteins are organic macromolecules built up from 20 different amino acids linked together by peptide bonds. Proteins are responsible for various functions such as forming part of extracellular matrix (ECM) for structural and mechanical support, cell signaling, and immune response and cell adhesion. Protein adsorption is a highly complex process. Protein adsorption can only take place if the Gibbs energy of the system decreases [12,13]. Proteins are surface-active and tend to accumulate at interfaces between the solid surface and liquid. Fig. 1.5 shows the schematic explanation of individual steps involved in the adsorption process of a protein molecule. The process and mechanism of protein adsorption and desorption can be explained as follows:

1. The protein molecules are transported from the solution towards the surface by diffusion and convection, influenced by solid surface electrostatic potential.
2. Protein attachment is driven by the decrease of the Gibbs energy in the system. The attachment of the proteins on the surface is influenced by their amino acid composition, size and their overall physical and chemical properties. The proteins also may change in structure upon adsorption
3. Interaction between the protein and surface might further alter the proteins' structure.
4. Desorption and the diffusion back into the solution might occurs although it is less probable due to high number of interaction points with the surface and a more stable binding after protein unfolding.

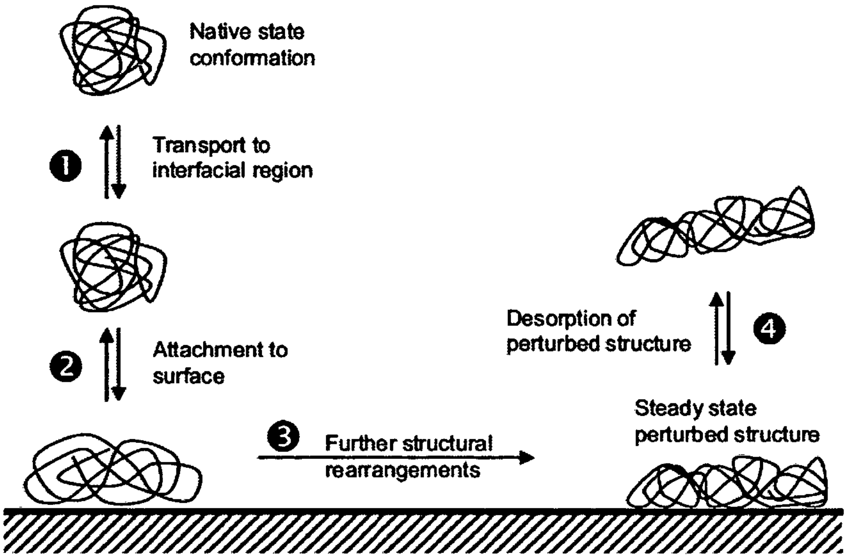
Native state conformation
❶ Transport to interfacial region
❷ Attachment to surface
❸ Further structural rearrangements
Desorption of perturbed structure ❹
Steady state perturbed structure

Fig. 1.5 Schematic representation of the process of protein adsorption on a solid surface [14].

Albumin is one of the most popular proteins in the human blood plasma while vitronectin is one of the key proteins for cell attachment onto the substrate surface in vitro cell culture condition. It is reported that albumin adsorption onto a material surface reduces the pro-inflammatory activity of macrophage [15] and platelet-activated thrombogenesis [16]. Vitronectin is a glycoprotein present in plasma mediating cell adhesion to a substrate surface [17] and reorganizing cytoskeleton [18].

1.3 Surface Characterization

1.3.1 Surface characterization

Key factors in determining good compatibility between the material and the host tissue are surface wettability, roughness, chemical composition, electric charge and mobility, and corrosion resistance [19]. Atoms on the surface are mostly highly unstable leading to enhanced mobility and higher reactivity. These surface atoms can easily undergo phase transformation, segregation or even dissolution (corrosion). Thus, surface characterization of the biomaterial is important in determining its biocompatibility.

1.3.2 X-ray Photoelectron Spectroscopy

X-ray photoelectron spectroscopy (XPS) is a standard tool used in characterizing the biomedical surface. XPS method is based upon the photoelectric effect in which soft X-rays are used to excite core and valence electrons within the atoms of a surface. As the X-rays are focused upon a sample, the interaction of the X-rays with the atoms in the specimen causes the emission of the core level electron. If the X-ray energy is large enough photoelectrons are expelled from the material and their kinetic energies (KE) are measured by the instrument. This excitation process is known as the photoelectric effect and is illustrated in Fig. 1.6. Differences in chemical elements within the near surface region are identified on the basis of their binding energy (BE), which is measured relative to the Fermi level (E_{Fermi}) of the individual atoms. The KE and BE of the photoelectron are related via the following equation:

$$KE = hv - BE - \phi_{spectrometer} \quad \text{(Eqn. 1.1)}$$

where hv represents the energy of the absorbed photon and $\phi_{spectrometer}$ is the work function of the spectrometer.

One of the key features of XPS is that both elemental and chemical information are easily available. This allows XPS to provide information on the oxidation state and local bonding environment of atoms within a surface layer. Due to the high elemental sensitivity of XPS, changes in oxide chemistry can be monitored. The XPS also can be use to differentiate between atoms that have different bonding arrangements to allows for the quantitative analysis of surfaces. Not only that, XPS can be used for depth analysis and as a result, the thickness or structure of oxide overlayer can be visualized.

From the XPS survey spectrum, the elemental concentration of a surface containing two or more elements (except for H and He) can be determined using the following formula:

$$X_A = (I_A/S_A)/(\Sigma_N(I_N/S_N)) \quad \text{(Eqn. 1.2)}$$

where X_A, I_A and S_A represent the atomic concentration (in at%), the peak area and the relative sensitivity factor (RSF) for element A in a surface having n elements, respectively. Any contributions of the energy loss background to the photoelectron peak intensities are removed using a subtraction algorithm [20].

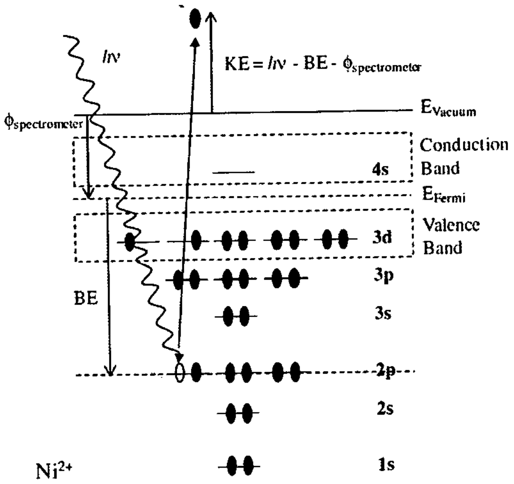

Fig. 1.6 An electron energy diagram for a Ni^{2+} showing the absorption of a photon and resultant expulsion of a 2p level photoelectron.

1.4 Corrosion in biomaterial

Medical implants based on metals are mainly used in load bearing application such as joint replacement, for the fixation of bone fracture, or mechanical support for enlarged tubular organs such as arteries vessels in form of screws or stents. Also, metal is widely used in the field of oral surgery. The mechanical properties of metals such as high strength and stiffness allowed for their usage over a long time. The biocompatibility of metal is depending on its good corrosion resistance to avoid impairment of the material properties due to degradation. Corrosion and wear resistance plays a major role as the host tissue may be damaged from the leaking corrosion products or abrasive particles.

Although carcinogenesis by metal prostheses is extremely rare in humans, however there are concerns regarding the possibilities of carcinogenic hazard. Several epidemiological studies have demonstrated the carcinogenicity of several metallic alloys such as nickel, cobalt, chromium or lead compounds. Metal particles produced by mechanical wear or metal ions released by corrosion might be initiating factors for such malignancies [21]. Wear debris is not biologically inert as their accumulation in local tissue is associated with chronic inflammatory reaction, although the nature of which depends on the type or size of the particle [22], concentration and duration of exposure [23], and the surface characteristic of the implants [24].

Although metal used as an implant is typically inert due to their good corrosion resistance, the complexity of biological environment might alter their corrosion behavior. Upon insertion into host, these implants encounter different environment with complex physio-chemical nature and their interaction with tissues and body fluid further complicating the corrosion behavior [25]. The corrosion of metallic biomaterials also is a multifactorial factor that depends on the geometric, metallurgic and solution-chemistry parameters [26].

1.4.1 General concept of corrosion

Metal implant corrosion is controlled by (1) the extent of the thermodynamic driving forces which cause corrosion (oxidation/reduction reactions) and (2) physical barriers which limit the kinetics of corrosion [27]. The two parameters will be discussed in detail as below.

(1) Thermodynamic consideration on metallic corrosion

The most relevant form of corrosion related to metallic biomaterials is aqueous corrosion. The electrochemical reaction happens when the metallic biomaterials is exposed to the aqueous electrolyte. Two basic reactions that occur during corrosion are anodic reaction and cathodic reaction. Anodic reaction is the increase of the valence state of the metal atom in which the metal loses electrons during anodic reaction.

$$M \rightarrow M^{n+} + ne^-$$

In cathodic reaction, the electron is consumed during the reaction. Depending on the nature of the electrolyte, the two most important reactions are the (1) reduction of hydrogen:

$$2H^+ + 2e^- = H_2$$

and (2) the reduction of dissolved oxygen:

$$O^{2-} + 4H^+ + 4e^- = 2H_2O \text{ (in acidic solutions)}$$

$$O^{2-} + 2H_2O + 4e^- = 4OH^- \text{ (in neutral or basic solution)}$$

For corrosion to occur, there must be a thermodynamic driving force for the oxidation of metal atoms. This driving force can be quantified thermodynamically using the Gibbs function, or free energy equation (the Gibbs function incorporates both the entropy and enthalpy changes of the above chemical reaction, or the total work to reach equilibrium).

At equilibrium, the chemical energy balances with the electrical energy, which can be quantified using the Nernst equation, which defines the electrical potential across an idealized metal–solution interface when in a solution.

$$E = E_0 + \frac{RT}{nF}\ln\frac{a_{anodic}}{a_{cathodic}} \quad \text{(Eqn. 1.3)}$$

where E_0 is the standard electrode potential, R is the gas constant, T is absolute temperature, F is the Faraday constant, n is the number of electrons transferred, and a_{anodic} and $a_{cathodic}$ is the activities (concentrations) of the anodic and cathodic reactants.

At low concentrations, the activity can be approximated to the concentration. In this situ- ation, there is a net dissolution of the metal and a current will flow. At equilibrium, the rate of the metal dissolution is equal to the rate of the cathodic reaction, and the rate of the reaction is directly proportional to the current density by Faraday's law; therefore:

$$i_{\text{anodic}} = i_{\text{cathodic}} = i_{\text{corrosion}} \quad \text{(Eqn. 1.4)}$$

and the Nernst equation can be rewritten:

$$E - E_0 = \pm\beta \ln(i_{\text{corr}}/i_0) \quad \text{(Eqn. 1.5)}$$

where β is a constant and i_0 is the exchange current density, which is defined as the anodic (or cathodic) current density at the standard electrode potential. Current density is the current, measured in amperes, normalized to the surface area of the metal.

(2) Kinetic barrier formation of oxide films

The second primary factor that influences the corrosion process of metallic biomaterials is the formation of stable surface barriers or limitations to the kinetics of corrosion. The barriers prevent corrosion by physically limiting the rate at which oxidation or reduction processes can take place. One example of kinetic limitation to corrosion is the formation of metal oxide passive film on a metal surface. In general, the passive films prevent the migration of metallic ions from the metal to the solutions, the migration of anions from solution to metal, or the migration of electrons across the metal–solution interface[28]. In order to limit oxidation, passive films must have certain characteristics. They must be non-porous and must fully cover the metal surface.

Passivating oxide films spontaneously grow on the surface of metals such as titanium alloys or stainless steels. These oxide films are generally very thin (on the order of 5 to 70 Å) and may be amorphous or crystalline. One of the more widely accepted models, by Mott and Cabrera [29], states that oxide film growth depends on the electric field across the oxide. The film will change its thickness by growth or dissolution until the rates of both are equal, giving rise to a film thickness that is dependent on metal oxide solution potential. If the interfacial potential is made sufficiently negative or the pH of the solution is made low enough, then these oxide films will no longer be thermodynamically stable and will undergo reductive dissolution, or there will be no driving force for the formation of the oxide, and the metal surface will become unprotected.

1.4.2 Corrosion resistance of TiNi alloys

The biocompatibility of TiNi alloys is derived from the passive titanium oxide (TiO_2) layer on the surface of the alloys. This layer acts as a barrier between the bulk TiNi and the human body. The formation of TiO_2 in the air is due to the low formation energy of TiO_2 in comparison to NiO. Titanium has a four-fold greater affinity for oxygen than nickel [30]:

$$Ti_{(s)} + O_{2(g)} \rightarrow TiO_{2(s)}\text{ , } \Delta H = -956 \text{ kJ/mol} \qquad \text{Eqn. 1.6}$$

$$Ni_{(s)} + \tfrac{1}{2}\, O_{2(g)} \rightarrow NiO_{(s)},\ \Delta H = -241 \text{ kJ/mol} \qquad \text{Eqn. 1.7}$$

As the oxide formation is favored thermodynamically, the passive layer on the TiNi alloys were mainly consists of TiO_2 despite the high nickel content [31]. The strongly adherent surface layer of 2-10 nm thickness were generally observed [32-34]. Furthermore, the oxide layer is spontaneously regenerated in milliseconds even after damage which is considered as an advantage for the biomedical application of Ti-based alloys [35].

The presence of cells is shown to have a detrimental effect to the protectiveness of the metallic biomaterial passive films. Fig. 1.7 shows a scheme of the effect of the fibroblast on the corrosion behavior of metallic biomaterial. In the study by Hiromoto et. al, they have found that the presence of fibroblasts increases the passive current density and decreases the pitting potential [36]. The pH near the cells was also found to be lower than that of the bulk medium due to the accumulated dissolved metal ions near the cells. The decrease of the pH level of the medium near the cells leading to the initiation of crevice corrosion that will affect the structural integrity of the metallic implant.

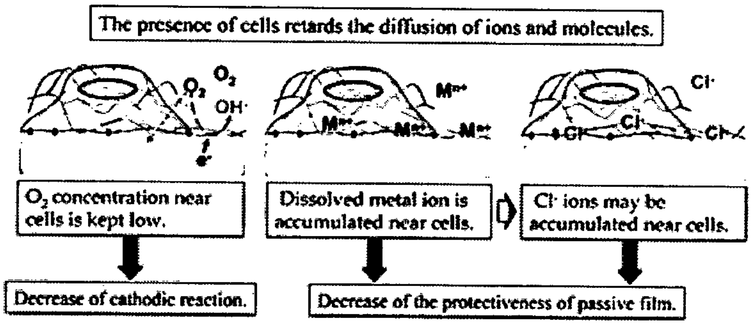
The presence of cells retards the diffusion of ions and molecules.
O₂
OH⁻
e⁻
Mⁿ⁺
Cl⁻
O₂ concentration near cells is kept low.
Dissolved metal ion is accumulated near cells.
Cl⁻ ions may be accumulated near cells.
Decrease of cathodic reaction.
Decrease of the protectiveness of passive film.

Fig. 1.7 Influence of fibroblast on the corrosion of biometallic material [37].

1.4.3 Ni ion release

Metal ion release has been often recognized as a cause of clinical failure or allergic reaction of metallic medical devices [38]. Measureable amounts of the metallic ions have been obtained in the tissues surrounding the implants as well as in the serum, body fluids, and urine [39]. For implanted Ni-containing alloys, wide variation in Ni ion release rate has been reported. The rate of Ni release range from 0.81-0.0081 mg/h per kilogram body weight totaling 5-500 mg/y for a 70 kg individual [40]. Ni ion release has been associated with carcinogenic, mutagenic, cytotoxic and allergenic reaction in the average patients [31,41]. The average percentages of metal sensitivity are approximately 10% for the general population, 22% for patients with well-functioning implants, and 60% for the patients with poorly functioning implants [42].

Although TiNi alloys are generally considered as biocompatible, nickel ion release can still be a problem. Presence of Ni within the oxide layer can lead to release of nickel ions into the surrounding media [43]. The formation of the oxide layer may result in the creation of a nickel-rich sublayer which can act as reservoirs of nickel ion release in the body as the nickel atoms are smaller than titanium and oxygen atoms, thus which allows the nickel atom to diffuse interstitially through surface oxide layers [44]. Various studies have been made to modify the surface structure of TiNi alloys to prevent Ni ion release into the surrounding such as by laser surface treatment [45], oxidation [46,47] or chemical passivation [34]. These findings emphasize the importance of controlling the nature and homogeneity of the TiNi oxide films.

1.5 Severe plastic deformation

Bulk nanostructured materials have gaining more interest in recent years due to its improved mechanical properties. Bulk nanostructured metals and alloys by severe plastic deformation have been seen as new alternative in producing nanocrystalline materials. Previously, in achieving grain refinement in metal and alloys, available techniques are mechanical alloying, inert gas condensation, and electrodeposition. However, in recent years there are growing interests in fabrication of bulk nanostructured materials by using severe plastic deformation (SPD). SPD process is currently defined as "any method of metal forming under an extensive hydrostatic pressure that may be used to impose a very high strain on a bulk solid without the introduction of any significant change in the overall dimensions of the sample and having the ability to produce exceptional grain refinement."[48].

1.5.1 Equal-channel angular pressing (ECAP)

In ECAP processing, a simple shear strain is introduced when the billet passess through the plane where the two channels meet. As the cross section of the billet remains unchanged, the billet can be repetitively go through the pressing, leading to accumulation of very large strain.

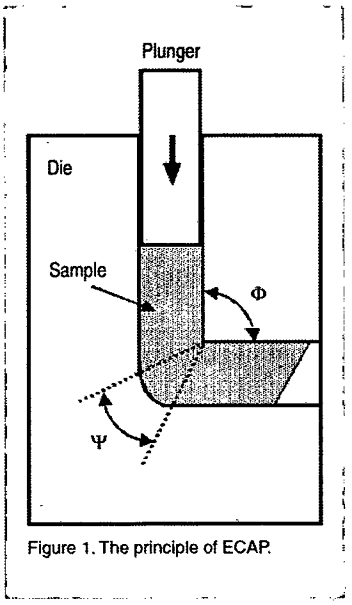

Fig. 1.8 Schematic of ECAP process [48]

1.5.2 Accumulative roll bonding (ARB)

In ARB process, the metal sheet is rolled to 50% thickness reduction. Then, the rolled sheet is cut into two and both halves are stacked together, thus restoring the original thickness of the sheet. The stacked sheet then were rolled together to half of the thickness. The repeating of rolling, cutting and stacking ultimately accumulated a large strain in the sheet [49].

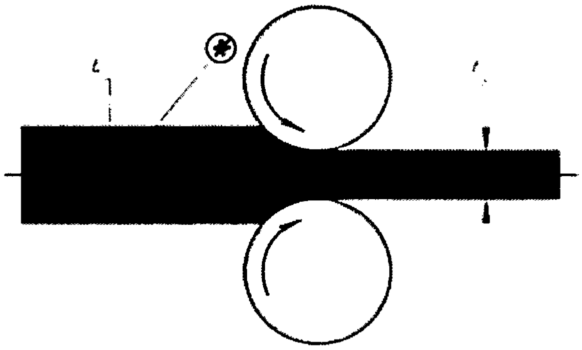

Fig. 1.9 Schematic of ARB process [49].

1.5.3 Multi-directional forging (MDF)

The principle of MDF is illustrated in Fig. 1.10 and it assumes multiple repeats of free-forging operations including setting and pulling with changes of the axes of the applied load. Multiple free-forging operations include repeated setting in three orthogonal directions. Since MDF is commonly performed in the temperature interval of 0.1– 0.5T_m, where T_m is the melting temperature, grain refinement during MDF is usually associated with dynamic recrystallization [50]. This method can be used to obtain a nanostructured state in rather brittle materials because processing starts at elevated temperatures and the specific loads on tooling are relatively low.

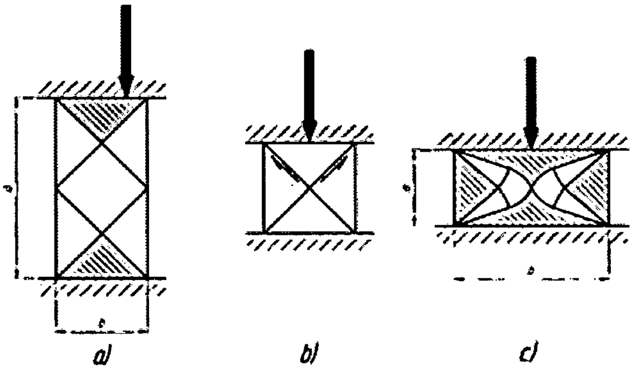

Fig. 1.10 Schematic of MDF process [50].

1.5.4 High pressure torsion

High-pressure torsion (HPT) is one of the SPD methods that have been used to produce bulk amorphous and nanostructured materials. During deformation by HPT, a sample is subjected to shear straining under a high quasi-hydrostatic pressure between two anvils, leading to grain refinement and amorphization of the sample, producing nanostructured material with improved mechanical properties [51]. This technique has a limitation on the dimensions of the samples compared to other SPD technique. However, it may be useful for applications in miniaturized implants or biomedical devices. In this process, the mechanical properties of the materials can be altered by controlling the degree of deformation i.e. the number of rotation.

The principle of HPT processing is depicted schematically in Fig. 1.11. The samples is located between two anvils where it is subjected to compressive applied pressure, *P*, of several GPa and simultaneously it is subjected to a torsional strain which is imposed though rotation of the lower anvil. As a result of high imposed pressure, the deforming sample does not break even at high strains. Due to high shear strain imposed on the sample during HPT deformation process, HPT can be used to produced bulk samples with up to nanometer size grains (down to <30nm) which is beneficial to produce small, disc-shaped samples for fundamental studies on nanostructured materials.